

# Semiempirical Model of Soil Water Hysteresis

John R. Nimmo\*

## ABSTRACT

In order to represent hysteretic soil water retention curves accurately using as few measurements as possible, a new semiempirical model has been developed. It has two postulates related to physical characteristics of the medium, and two parameters, each with a definite physical interpretation, whose values are determined empirically for a given porous medium. One parameter represents the fraction of the pore space that is not subject to Haines jump hysteresis. Its associated postulate is that a single value of this parameter characterizes a given medium, or, equivalently, that the medium is self-similar with respect to the division between hysteretic and nonhysteretic pore space. The second parameter is the effective body-to-neck size ratio of the medium's largest pore. The second postulate specifies a particular relation between the size distributions of pore bodies and of pore necks. Tests of the model show that it provides high-quality optimized fits to measured water content vs. matric pressure wetting curves for a wide variety of media. The parameter values obtained through optimization correlate plausibly with such media properties as uniformity of particles, complexity of structure, and degree of compaction. A practical use of this model is to provide a complete simulated main wetting curve for a medium where only a main drying curve and two points on the wetting curve have been measured. With additional development, it may be possible to do without the two measured wetting points if parameters can be evaluated from other measurements or known properties of the medium.

WHERE both drying and wetting occur during an unsaturated flow process, quantitative analysis generally must take into account the hysteresis of soil water characteristics. Considering the water content ( $\theta$ ), matric pressure ( $\psi$ ), and hydraulic conductivity ( $K$ ), the  $\theta$ - $\psi$  and  $K$ - $\psi$  relations are always hysteretic. The common assumption of negligible  $K$ - $\theta$  hysteresis increases the importance of  $\theta$ - $\psi$  hysteresis, as it then becomes the sole determinant of  $K$ - $\psi$  hysteresis. Unless measurements have been made of all the families of  $\theta(\psi)$  curves needed for a given calculation, one must rely on a model that represents a complete hysteretic relation, given an incomplete data set.

Domain models of hysteresis are the most widely used for soil water calculations. Néel (1942, 1943) developed the first of these, not for porous media but for hysteresis of magnetization of a material in which there are tiny domains of a particular magnetic ori-

entation. Everett (1955) and Enderby (1955) extended and generalized this type of model. The adaptation for soil water involves a substitution of pores for magnetic domains. The pores empty and fill in response to changes in applied pressure just as the orientation of magnetization changes in response to changes in the applied magnetic field. Much of the emptying and filling of pores occurs in sudden jumps (Haines, 1930), accounting for the hysteresis of soil water as explained in detail by Miller and Miller (1956). Pouloussis (1962) employed these ideas in a domain model analysis of measured  $\theta$ - $\psi$  hysteresis.

The direct incorporation of similarity hypotheses into domain models by Philip (1964) and Mualem (1973) improved the representation of soil water hysteresis. This work led to the practical and widely applicable model of Mualem (1974), sometimes referred to as Model II, which has successfully represented scanning curves for a variety of porous media. The development of dependent domain models (Mualem and Dagan, 1975) provided a means of allowing for pore "blocking" — the prevention of sudden changes in a pore's water content by elimination of water or air pathways to the pore — which may be important in some media.

The main shortcoming of models like Mualem's Model II is that they require measurements of complete main wetting and drying curves. Such a complete data set is seldom available, and by most techniques the wetting curve in particular is difficult or time-consuming to measure. Another disadvantage is that the hysteresis is represented in terms of characteristic functions, not all of which can be easily related to other physical properties.

To get by with a smaller data set, Parlange (1976) and Mualem (1977, 1984) developed models that require only a main drying curve to represent a main wetting curve and all scanning curves. These models work tolerably well for some but not all soils. Given a medium with a measured drying curve only, it cannot be predicted whether a model of this type will represent hysteresis of that medium with acceptable accuracy. This problem makes such models impractical for most situations. On a fundamental level, moreover, there is no significant evidence that the phenomena that cause hysteresis are manifested in a main drying curve.

I propose a semiempirical model that has been designed to provide a good representation of a main

Water Resources Division, U. S. Geological Survey, MS-421, 345 Middlefield Rd., Menlo Park, CA 94025. Received 27 Aug. 1991. \*Corresponding author.

wetting curve, given a main drying curve and as little additional information as possible. This model requires fewer data than Model II, though more than the drying-curve-only models. To reduce the reliance on plentiful data, such a model must incorporate assumptions that can represent the most important of the phenomena that determine hysteresis.

A second objective of the model is to represent hysteresis in terms of parameters with a definite physical interpretation. If there is a sound basis for this interpretation, the particular values that such parameters take on can provide insight into the mechanisms of pore-water interactions.

### STRUCTURE OF THE MODEL

The model's basic framework is similar to that of most other models of soil water hysteresis. Of the possible mechanisms, it assumes Haines jumps to be dominant. Although other mechanisms, such as contact-angle hysteresis, also contribute to soil water hysteresis, they may be negligible in comparison. The best support for this assumption is in the success of models (e.g., Mualem, 1974) that are based on the Haines jump mechanism. The model presented here treats only the repeatable portions of the hysteretic relation. That is, it applies not to an initial drying curve, which starts from complete saturation, but to curves that include the effects of trapped air such that both drying and wetting curves have the same maximum  $\theta$ . To model the initial drying curve requires consideration of a quite different set of phenomena, so it is best treated with a separate model as was done by Mualem (1974). The terms *main drying* and *main wetting* designate curves between  $\theta$  and the minimum water content of retention measurements, and *scanning* designates curves whose starting water content is between these extremes. Each pore is considered to have a characteristic pressure ( $\psi_d$ ) at which it largely empties and a greater characteristic pressure ( $\psi_w$ ) at which it largely refills. The radius of curvature ( $r$ ) of an air-water interface is taken to be inversely proportional to  $\psi$ . Then  $\psi_d$  and  $\psi_w$  are also inversely proportional to the effective drying and wetting radii ( $r_d$  and  $r_w$ ). The radius  $r_d$  is considered to indicate the size of the pore neck and  $r_w$  the size of the pore body.

The model's two parameters are each associated with a physical property of porous media that affects hysteresis and with a visible feature of a graphed hysteretic relation.

The first parameter, symbolized  $\nu$ , relates to the fact that not all pore space is subject to Haines jump hysteresis. Some fraction of the pore space, including dead-end pores, films coating surfaces, and some of the space within hysteretic pores, does not drain or refill by Haines jumps. The parameter  $\nu$  is defined as the fraction of the  $\theta_{\max}$  pore space that is nonhysteretic. In general it might depend on  $\psi$  and  $\theta$ , as there might be more or less nonhysteretic space in the small pores that are filled at low  $\theta$  than in the large pores that are filled at high  $\theta$ . Another possibility is that  $\nu$  itself may depend on the history of drying and wetting events, but here I assume it does not. To visualize the effect of  $\nu$  on a water-retention graph, refer to Fig. 1, considering the slopes  $\theta'_d$  and  $\theta'_w$  at the point of drying-wetting reversal ( $\psi_{\text{rev}}$ ). If  $\nu$  has a value close to one, hysteresis is minimal, the wetting curve is close to the drying curve, and the slopes  $\theta'_d$  and  $\theta'_w$  are approximately equal. If  $\nu$  has a value close to zero, then hysteresis is maximal, and  $\theta'_w$  is approximately zero. While an exact relation between  $\nu$  and this slope ratio is not possible for real data because some Haines jumps would normally affect  $\theta'_w$  as well as  $\theta'_d$ , the ratio  $\theta'_w/\theta'_d$  at  $\psi_{\text{rev}}$  clearly increases as  $\nu$  increases.

The second parameter, symbolized  $\beta$ , represents the body-

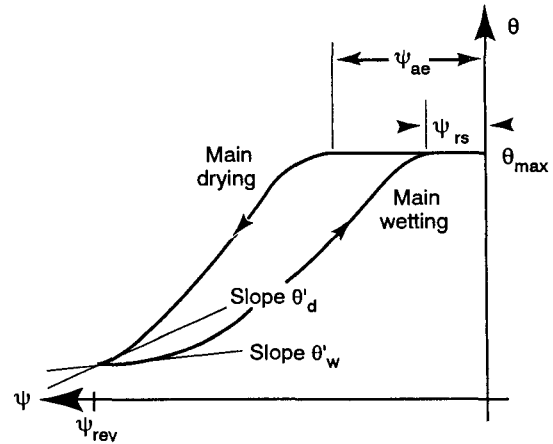


Fig. 1. A typical hysteretic main-curve water retention relation, with water content symbolized by  $\theta$  and matric potential by  $\psi$ . The nonhysteretic-space parameter  $\nu$  is greater for large values of the ratio of slopes  $\theta'_w/\theta'_d$ . The pore-geometry parameter  $\beta$  is greater for large values of the ratio of air-entry value to resaturation value,  $\psi_{ae}/\psi_{rs}$ .

to-neck size ratio ( $r_{w-\max}/r_{d-\max}$ ) of the biggest pore that refills with water. Since radii are inversely proportional to  $\psi$ ,  $\beta$  equals the ratio of the air-entry value ( $\psi_{ae}$ ) to the resaturation value ( $\psi_{rs}$ ), as illustrated in Fig. 1. For media with both  $\psi_{ae}$  and  $\psi_{rs}$  close to zero,  $\beta$  may become ill defined. The model can still be applied, but would be expected to have little sensitivity to  $\beta$ .

Because the model treats repeatable hysteresis loops but not initial drying curves, the terms *air-entry* and *resaturation* apply analogically rather than literally. In reality, some air is always present in the soil. A  $\theta(\psi)$  curve may approach, but not quite equal, zero slope. Thus where a precise mathematical determination is necessary, the departure of  $\theta(\psi)$  from  $\theta_{\max}$  is not a suitable criterion. One alternative is the point of maximum curvature of  $\theta_d(\psi)$ , which often gives values close to what would be selected as  $\psi_{ae}$  by eye.

The first of the two hypotheses that relate  $\nu$  and  $\beta$  to the entire hysteretic relation is that the fraction of pore space that is nonhysteretic is independent of pore size. In other words, a single  $\nu$  value, independent of  $\psi$  or  $\theta$ , characterizes a medium. This hypothesis implies a self-similarity of the pores with respect to the degree to which they are nonhysteretic. Various soil physical properties may be self-similar to a significant degree, as has been suggested by Tyler and Wheatcraft (1989) and Toledo et al. (1990), though the extent and cause of this phenomenon require further exploration.

The second hypothesis concerns pore-size distributions. Following convention (Childs and Collis-George, 1950), the pore-neck size distribution function  $f_d(r)$  is related to the main drying curve  $\theta_d(r)$  according to

$$\theta_d(r) = \int_0^r f_d(\bar{r}) d\bar{r} \quad [1]$$

and correspondingly

$$f_d(r) = d\theta_d/dr. \quad [2]$$

Applying the constant- $\nu$  hypothesis, the distribution of nonhysteretic pores is  $\nu f_d(r)$ . Plotting both  $f_d(r)$  and  $\nu f_d(r)$ , as in Fig. 2, divides the represented pore space into hysteretic and nonhysteretic portions (H space and N space) in which the area enclosed by a curve is proportional to pore volume. Pores with  $r_d$  equal to an arbitrary  $\bar{r}$  can be represented by

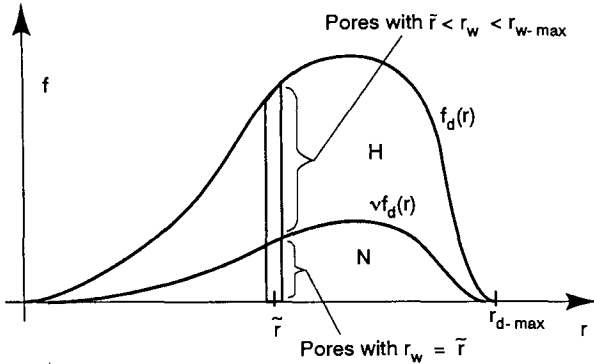


Fig. 2. Example, for a typical soil with nonhysteretic-space parameter  $\nu = 0.3$ , of the total pore-size distribution function  $f_d(r)$  and nonhysteretic pore-size distribution function  $\nu f_d(r)$ , where  $r$  is the effective pore neck radius. The curve  $\nu f_d(r)$  divides this diagrammatic representation of pore space into hysteretic (H) and nonhysteretic (N) portions.

an infinitesimally thin vertical strip at  $r = \tilde{r}$ , as diagrammed in Fig. 2. The  $r_w$  values of these pores range from  $\tilde{r}$  to  $r_{w-max}$ . If these pores are thought of as being arranged vertically in ascending order of body size, the nonhysteretic pores with  $r_w = r_d = \tilde{r}$  would occupy the N-space portion between zero and  $\nu f_d(\tilde{r})$ . The hysteretic pores would be arranged with  $r_w$  increasing from  $\tilde{r}$  at  $\nu f_d(\tilde{r})$  to  $r_{w-max}$  at  $f_d(\tilde{r})$ . The second hypothesis specifies the body-size distribution of these H-space pores, making use of a function  $f_{str}(\tilde{r}, r)$  illustrated in Fig. 3. The portion of  $f_d(r)$  between  $\tilde{r}$  and  $r_{d-max}$  is stretched linearly in the  $r$  direction to cover the region between  $\tilde{r}$  and  $r_{w-max}$ , defining  $r_{w-max}$ . Then the body-size distribution of H pores with neck size  $\tilde{r}$  is taken to be proportional to  $f_{str}(\tilde{r}, r)$ . The proportionality constant must be given the value that normalizes computed  $\theta$  values, as shown below. The function  $f_{str}$  is algebraically related to  $f_d$  as

$$f_{str}(\tilde{r}, r) = f_d([r - \tilde{r}]/\alpha + \tilde{r}) \quad [3]$$

where the stretching factor  $\alpha$  is

$$\alpha = \frac{r_{w-max} - \tilde{r}}{r_{d-max} - \tilde{r}} = \frac{\beta r_{d-max} - \tilde{r}}{r_{d-max} - \tilde{r}} \quad [4]$$

This hypothesis is physically plausible since the abundance of pore bodies of a certain size may correlate with the abundance of pore necks that are smaller by a systematic amount. Yet it is hard to justify by comparison with directly measurable properties. Its validity depends primarily on how well the model it defines fits measured data.

Figure 4 shows how the two hypotheses define the model. Again, this diagram has  $f_d(r)$  based on effective neck sizes, body sizes varying upward from small to large, and areas under the curve directly proportional to pore space or  $\theta$ . Main drying is represented by integration according to the definition of  $f_d(r)$  in Eq. [1]. After drying to  $\psi_{rev}$ ,  $\theta$  is proportional to the gray area to the left of  $r_{rev}$ . After rewetting to  $r_s$  from the reversal at  $r_{rev}$ ,  $\theta = \theta_w(r_s)$  on the main wetting curve is proportional to the sum of three shaded areas: (i) all pore space with  $r_d$  less than  $r_{rev}$  (gray area) remains filled; (ii) all of the N space between  $r_{rev}$  and  $r_s$  (dotted area) becomes filled. (N-space pores, having in effect equal values of  $r_d$  and  $r_w$ , refill immediately during any wetting event); (iii) the fraction of the H space between  $r_{rev}$  and  $r_s$  in which  $r_w < r_s$  (hatched area) becomes filled. The curve bounding the upper portion of the hatched area does not have a simple relation to the  $f_d(r)$  curve and is

shown hypothetically in the figure. This curve may be thought of as the locus of points for which  $r_w = r_s$ .

Unlike a Mualem diagram (Mualem, 1974), Fig. 4 includes the functions to be integrated, not just the  $r$  domain over which the integration is to take place. Areas are directly proportional to  $\theta$ . In determining the portion of Fig. 4 to be integrated, two rules are followed. A drying operation reduces the area to be integrated by sweeping a vertical line segment leftward through H and N space. A wetting operation increases the area by sweeping a vertical line segment rightward through N space only, and adding the portion of H space in which  $r_w < r$ .

The derivation of formulas for modeled curves follows from the integration of appropriate areas on a diagram like Fig. 4. For  $\theta_w(r)$  on a wetting curve, either main or primary scanning, the areas are as shown, indicating

$$\theta_w(r) = \theta_{rev} + \int_{r_{rev}}^{\min(r, r_{d-max})} [\nu + (1 - \nu)\gamma(\tilde{r}, r)] f_d(\tilde{r}) d\tilde{r} \quad [5]$$

The term  $\theta_{rev}$  is the gray area in the diagram, the integral of  $\nu f_d(\tilde{r})$  is the dotted area, and the remaining integral is the hatched area. To keep the integral within the domain for which  $f_d(r)$  is defined, the upper limit is constrained not to exceed  $r_{d-max}$  even when  $r$  exceeds  $r_{d-max}$ . The function  $\gamma(\tilde{r}, r)$  is defined as the fraction of H space at  $\tilde{r}$  that has  $r_w \leq r$ . In other words, considering a vertical line from  $\nu f_d(\tilde{r})$  to  $f_d(\tilde{r})$ , the fraction of its length within the hatched area is  $\gamma(\tilde{r}, r)$ .

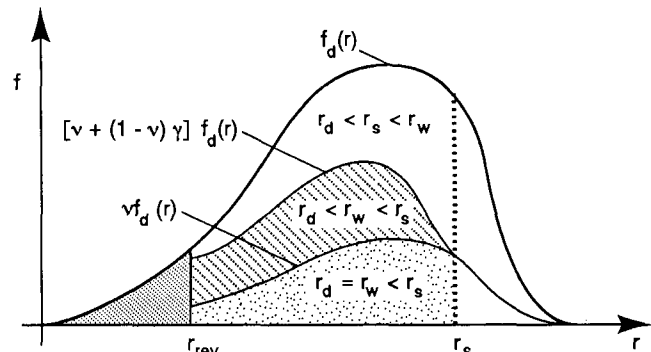


Fig. 3. A pore-size distribution function  $f_d(r)$  with the function  $f_{str}(r)$  relating to the size distribution of pore bodies for pores with neck radius  $\tilde{r}$ .

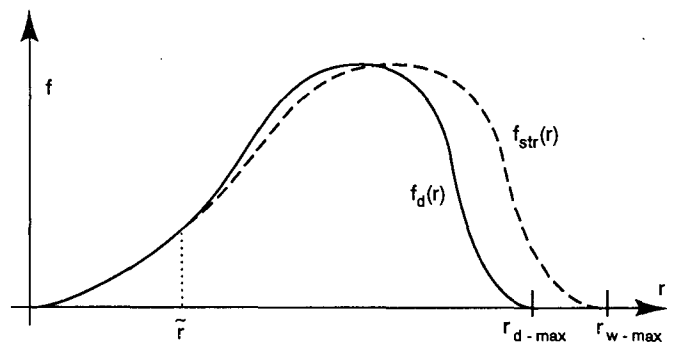


Fig. 4. Diagram illustrating the application of the model to the situation existing after drying to  $r_{rev}$  and then rewetting to  $r_s$ . The water content for this condition is proportional to the sum of the three shaded areas: the gray area that never was emptied, the dotted area with nonhysteretic space that refills at the same  $r$  values at which it emptied, and the hatched area with hysteretic space that refills at  $r \leq r_s$ .

The formulation of  $\gamma$  depends on the function  $f_{str}$  in Fig. 3. Of all the H space pores with  $r_d = \bar{r}$ , the portion that are filled is represented by the integration of  $f_{str}$  from  $\bar{r}$  to  $r$ , divided by the total integration from  $\bar{r}$  to  $r_{w-max}$ :

$$\gamma(\bar{r}, r) = \frac{\int_{\bar{r}}^r f_{str}(\bar{r}, r_w) dr_w}{\int_{\bar{r}}^{r_{w-max}} f_{str}(\bar{r}, r_w) dr_w} \quad [6]$$

Substituting Eq. [3] into Eq. [6] and applying the definition of  $f_d(r)$  from Eq. [1] yields

$$\gamma(\bar{r}, r) = \frac{\theta([r - \bar{r}]/\alpha + \bar{r}) - \theta(\bar{r})}{\theta_{max} - \theta(\bar{r})} \quad [7]$$

For practical use of the model,  $\psi$  values can be converted to effective  $r$  values using an assumed value of the constant of the inverse proportionality between  $r$  and  $\psi$ . This constant may have a value of about  $-130 \mu\text{m}\cdot\text{kPa}$  for typical soils, based on studies by Chen and Schnitzer (1978) and Tschapek et al. (1978) in which data interpreted as surface tension measurements of soil solution have an average of  $67 \text{ mN/m}$ . The data must be represented by a smooth curve so that  $f_d(r)$  can be computed by differentiation. Then Eq. [5], [7], and [4] yield  $\theta_w(r)$ . Alternatively, the model could be developed in terms of  $\psi$  rather than  $r$ , but  $r$  has the advantages of a finite valuation and a close conceptual relation to the geometric configurations that determine Haines jump hysteresis.

The model represents primary drying scanning curves and all higher order scanning curves by the principles used so far. Referring again to Fig. 4, any drying operation is represented by reducing shaded areas by a single vertical line segment sweeping leftward. For primary drying scans, this gives

$$\theta_{d1}(r) = \theta_{rev} + \int_{r_{rev}}^{\min(r, r_{d-max})} [\nu + (1 - \nu)\gamma(\bar{r}, r_s)] f_d(\bar{r}) d\bar{r} \quad [8]$$

Any wetting operation is represented by sweeping a vertical line segment rightward through N space and adding that portion of H space in which  $r_w < r$ .

### TESTING THE MODEL

The first tests of the model used measured data sets that included main drying and wetting curves, taking the drying curve as input data and determining  $\nu$  and  $\beta$  values that produced the best fits to the wetting curve. The two main objectives were to see how well the modeled curves could match the shape of the measured wetting curves and to see if the optimized parameter values were consistent with known properties of the test media.

The media used in these tests are listed in Table 1, roughly in order of increasing structural complexity. Of the published data sets that have both complete main curves, these were chosen mainly for variety. They include various textures, various temperatures, natural and artificial origin, consolidated and unconsolidated media, and one case of the same material packed to two different densities. One shortcoming of this list, reflecting the historical emphasis on repacked samples, is that only one medium (Plano silt loam) is a minimally disturbed soil core. Curves were fit to measured data points in different ways, depending on measurement technique. A modified least-squares polynomial fit, described by Nimmo (1983), was used for the  $\gamma$ -ray atten-

uation measurements of Nimmo and Miller (1986) and of Topp (1969, 1971). This type of curve was chosen to smooth out the scatter in the data while retaining several degrees of freedom for reasonably accurate curve shape. A monotonicity-preserving interpolant similar to a spline fit (Fritsch and Butland, 1984), as suggested by Stonestrom (1987), was used for the other media, which were measured by methods that produce a few high-quality data points. With the drying curves given, STARPAC algorithms (Donaldson and Tryon, 1983) were used to find the values of  $\nu$  and  $\beta$  that produce the optimal fit to the main wetting curves.

The results include mostly excellent fits, as listings in Table 1 and the representative selections shown in Fig. 5 indicate. The table lists optimum parameter values and the coefficient of multiple determination ( $R^2$ ), given as an indication of quality of fit (Draper and Smith, 1981, p. 90).

For one medium, Grenville silt loam of Staple (1965), the STARPAC optimization failed to converge properly. Trial and error tests of many parameter values produced only poor fits. The likely problem is that the curves for the medium (for which Staple shows the low- $\theta$  portion of the drying curve only by dashes, indicating a lower degree of confidence) have a high degree of hysteresis with  $\psi$  far from zero. For example,  $\theta_d$  and  $\theta_w$  differ by a factor of 1.5 at  $\psi = -1500 \text{ kPa}$ . Here, the equivalent  $r$  is about  $0.09 \mu\text{m}$  and it is unlikely that Haines jumps are the main cause of this hysteresis. As the model is based on the Haines jump mechanism, it may be simply inapplicable to situations where there is much hysteresis for  $\psi$  beyond a few hundred kilopascals.

For most media, the model reproduces the wetting curve closely. Plainfield sand (Fig. 5b) shows the best fit. Other minimally structured media (glass beads, silty sand) also fit well, the poorest fit of these being the lightly packed silty sand of Croney and Coleman (1954) shown in Fig. 5c. More complex soils, such as the Plano silt loam core sample, and consolidated media also fit well.

The modeled curves sometimes show an unwarranted wiggle where there is a sharp air-entry effect. This is seen clearly in Rubicon sandy loam (Fig. 5e) and, to a lesser degree, in Rideau clay loam. The tendency is for the sharpness of the bend in  $\theta_s(\psi)$  to echo somewhat in the modeled  $\theta_w(\psi)$  at about the same  $\psi$  values. This effect may reflect a departure of  $\nu$  from constancy near  $\psi_{ae}$ . The N space shown in Fig. 2 would probably be more accurately por-

Table 1. Optimized fits of the hysteresis model to main wetting curves.

Reference	Medium	$\nu$	$\beta$	$R^2$
Nimmo and Miller (1986)	Glass beads, 4 °C	0.06	2.26	0.996
	Glass beads, 20 °C	0.01	2.31	0.998
	Glass beads, 35 °C	0.04	2.51	0.997
	Glass beads, 50 °C	0.00	2.64	0.997
	Plainfield sand, 20 °C	0.52	2.2	0.997
	Plainfield sand, 35 °C	0.385	2.12	0.999
Croney and Coleman (1954)	Plainfield sand, 50 °C	0.464	2.41	0.998
	Silty sand, lightly packed	0.10	4.7	0.981
	Silty sand, densely packed	0.37	3.6	0.995
Topp (1969)	Rubicon sandy loam	0.33	8.3	0.988
Topp (1971)	Caribou silt loam	0.310	7.0	0.996
	Rideau clay loam	0.39	6.1	0.994
Croney and Coleman (1954)	Soft chalk	0.26	5.3	0.982
	Hard chalk	0.33	10.6	0.998
Nimmo and Miller (1986)	Plano silt loam, 4 °C	0.52	16	0.990
	Plano silt loam, 35 °C	0.48	24	0.987
	Plano silt loam, 50 °C	0.41	200	0.996
Staple (1965)	Grenville silt loam	0.0†	$2 \times 10^7$ †	0.614†

† Values listed for Grenville silt loam represent the best fit found in a manual trial-and-error search.

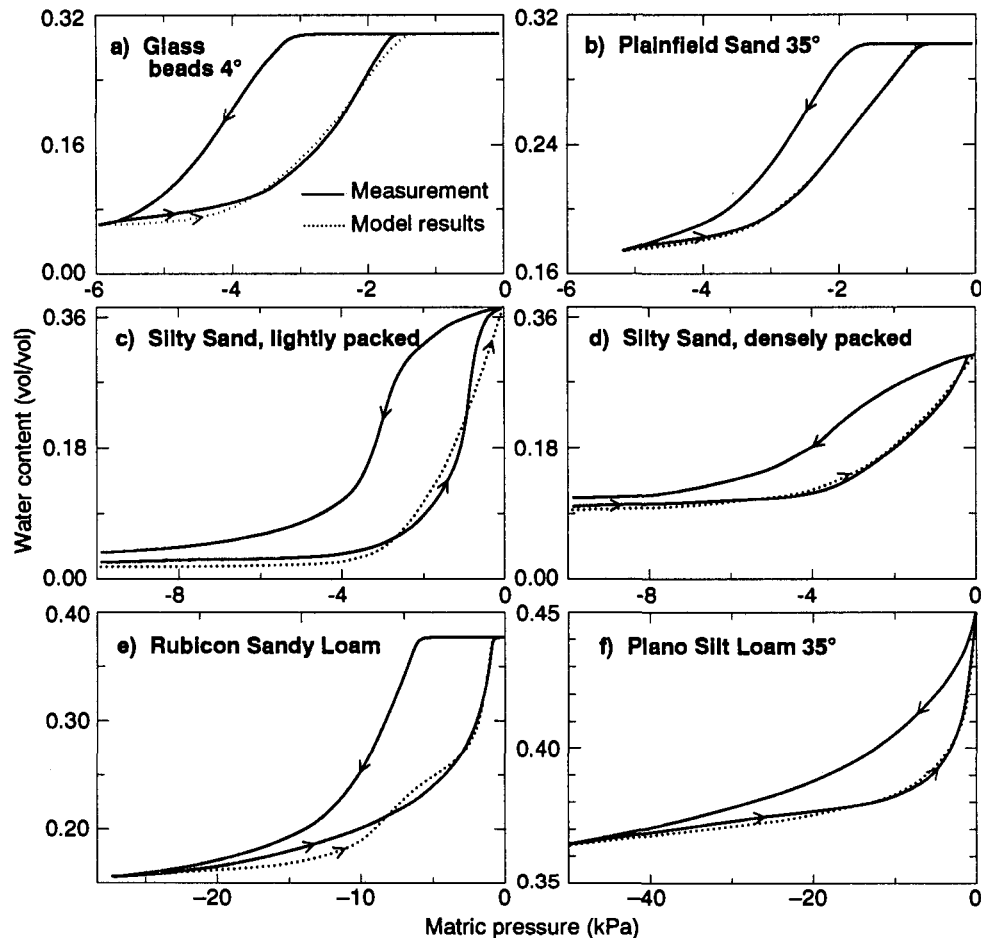


Fig. 5. Application of the model to the main wetting curves of six media. Dotted curves are computed using the optimized parameter values given in Table 1.

trayed as going to zero less abruptly as  $r$  increases to  $r_{d,max}$ . Even with constant  $\nu$ , though, this effect appears for only two of the media tested and the fit quality may be tolerable anyway. It is also worth noting that both of these media are repacked samples of soils that would normally have significant macropore structure in the field. The destruction of macropores in repacking probably creates the sharpness of the air-entry effect that diminishes the quality of the fit. In other words, the degree of self-similarity existing in a field soil might be reduced when the soil is repacked.

For glass beads,  $\nu$  is close to zero, as would be expected for a set of smooth-surfaced, regularly shaped, monodispersed particles. Pores that have necks smaller than their bodies, and thus are subject to Haines jumps, constitute nearly the entire pore volume of this medium. The natural media have more dead-end pores, particle-contact points, specific surface area, and other features likely to increase the nonhysteretic space, so it is reasonable that they also have greater  $\nu$ . Packing density also causes a substantial but expected effect: the more compacted silty sand of Cronney and Coleman (1954) (Fig. 5d) has much greater  $\nu$ , consistent with a reduction of large pores and an increase of particle contacts and closely parallel surfaces.

Several trends are apparent in the optimized  $\beta$  values in Table 1. The values are lowest for coarse, minimally structured media. The value of about 2.4 associated with these cases may indicate a characteristic minimum of the greatest body-to-neck ratio, applicable to a medium in which grains are ordered with a high degree of randomness, without sig-

nificant aggregation or macropore structure. Fine-textured media have greater  $\beta$  values, a probable result of the more complex structure that correlates with fineness. For the consolidated (chalk) samples,  $\beta$  was fairly large also, perhaps in part because the rigid pore structure may easily support greater ratios of body-to-neck size. Plano silt loam has the greatest  $\beta$  values and, in tests of quality of fit produced by a range of nonoptimized parameter values, it also proved to be fairly insensitive to the precise value of  $\beta$ . This insensitivity is consistent with the poorly defined relation of  $\psi_{ae}$  to  $\psi_{rs}$  when both are near zero (Fig. 5f). These facts suggest that, for a medium with significant macropore structure, the value of  $\beta$  is not strongly determined, but a large value works best. The general trend of optimized values shows an increase in  $\beta$  with greater structural complexity.

For the three media that have measurements at different temperatures, there is virtually no trend in parameter values with temperature. The lone exception is for  $\beta$  of Plano silt loam, the case of minimal sensitivity. In a further test of temperature dependence, arithmetic means of  $\nu$  and  $\beta$  values were computed for each medium and the resulting averages used to compute modeled wetting curves for each medium at each temperature. The resulting fits were good, the worst ones having  $R^2$  values of 0.990 for the beads, 0.997 for the sand, and 0.914 for the silt loam. This result implies a lack of substantial temperature dependence of the  $\nu$  and  $\beta$  parameters, in agreement with the conclusion of Nimmo and Miller (1986) that the magnitude of hysteresis does not depend on temperature.

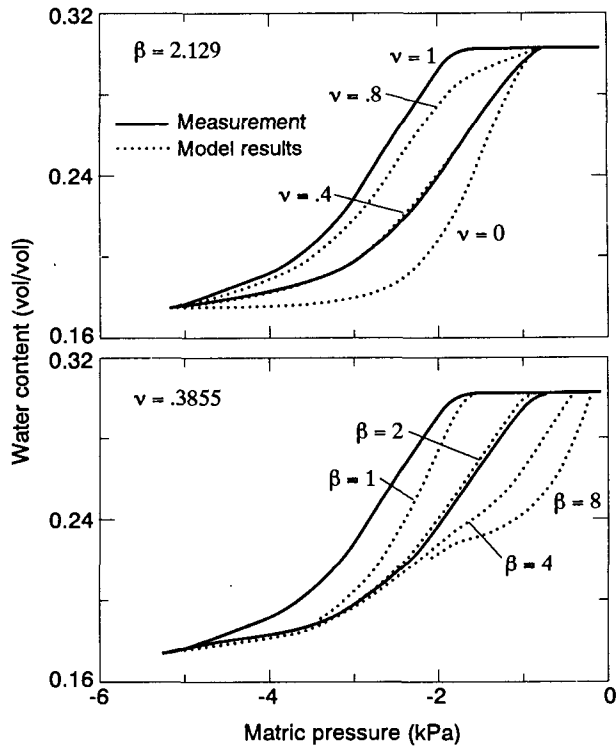


Fig. 6. The individual influences of the nonhysteretic-space parameter  $\nu$  and the pore-geometry parameter  $\beta$  on the modeled wetting curve of Plainfield sand at 35 °C, illustrating a particular case of the relations presented in Fig. 1.

Figure 6 illustrates the influence of each of the parameters. In Fig. 6a, four different  $\nu$  values (including  $\nu = 1$ ), paired with the same  $\beta$ , show the variation in slope at  $\psi_{rev}$  and its effect on the whole wetting curve. In Fig. 6b, four  $\beta$  values, paired with the same  $\nu$ , show the variation in the point at which the wetting curve rejoins the drying curve.

Although it is not its main purpose, this model can be used to compute scanning curves. This has been done for the media in Table 1 for which primary scanning data are available. Results show that it works best for the minimally structured media with low values of  $\beta$ . Figure 7 illustrates this, showing the best case of scanning curve fits, glass beads at 50 °C ( $\beta = 2.64$ ), and the worst case, Plano silt loam at 50 °C ( $\beta = 200$ ).

### PRACTICAL APPLICATION

The chief practical purpose for which the model was developed is reducing the number of measurements required for a complete hysteresis loop. Having two parameters, it can generate a main wetting curve to exactly fit two measured points. Table 1 and Fig. 5 show that it can accurately reproduce the shape of the main wetting curve for a wide variety of media. If this model can accurately generate the complete main wetting curve given only two measured wetting points in addition to the complete main drying curve, it can substantially reduce the time and effort required to obtain a complete, detailed hysteresis loop. This would be especially valuable when  $\theta(\psi)$  curves are measured using point-by-point equilibration methods (e.g., pressure plate, Tempe cell). Figure 8 shows an example in which values of  $\nu$  and  $\beta$  were determined with the criterion that the resulting modeled  $\theta_w(\psi)$

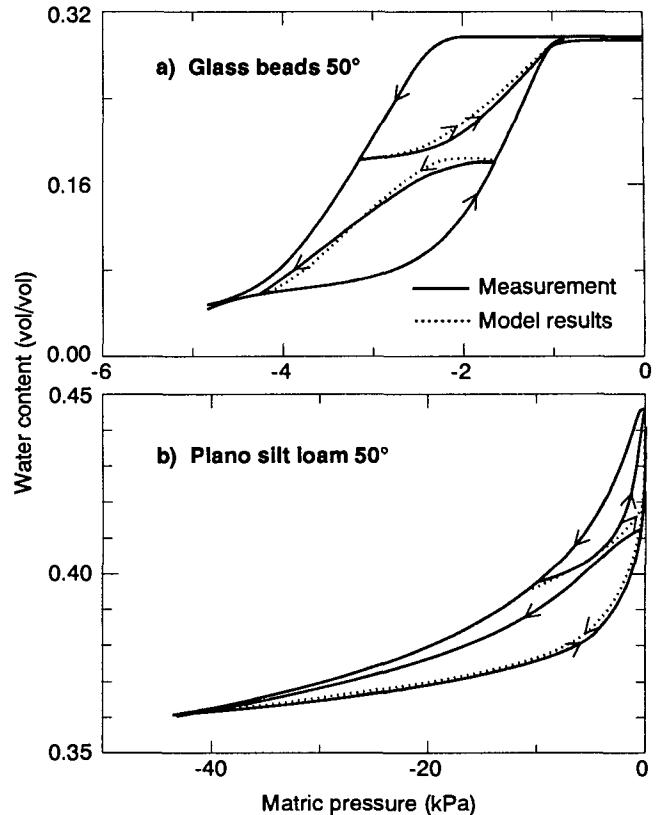


Fig. 7. Application of the model to scanning curves of glass beads at 50 °C and Plano silt loam at 50 °C. Dotted curves are computed using the optimized parameter values in Table 1.

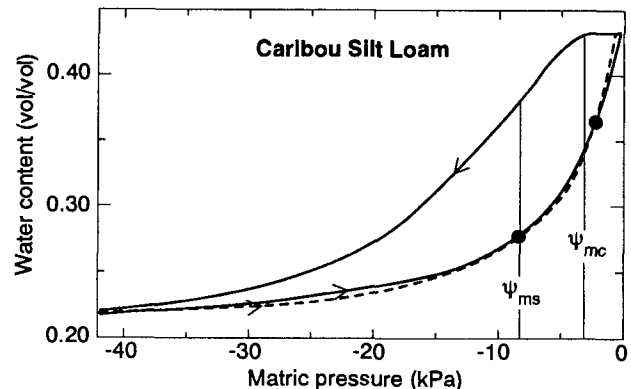


Fig. 8. Modeling the main wetting curve of Caribou silt loam with parameter values that constrain the curve to go exactly through two points, indicated by solid circles, on the measured wetting curve. These two points were taken at the matric potential ( $\psi$ ) value corresponding to the maximum slope of the main drying curve and at 0.9 times the  $\psi$  value corresponding to the point of maximum curvature of the main drying curve.

would exactly fit the measured curve at points corresponding to designated  $\psi$  values  $\psi_1$  and  $\psi_2$ . This was done using the Newton-Raphson method (Press et al., 1989, p. 269) to solve for the simultaneous root of the two nonlinear equations formed by equating the modeled and actual  $\theta$  values at  $\psi_1$  and  $\psi_2$ .

In applying the model for this purpose, after the

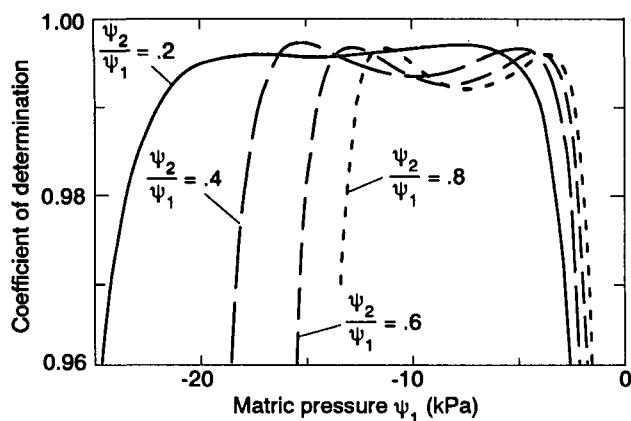


Fig. 9. Coefficients of multiple determination for modeled main wetting curves compared with measured main wetting curves for Caribou silt loam, the modeled wetting curve being forced exactly through two measured points at matric potentials  $\psi_1$  and  $\psi_2$ .

drying curve has been measured, the main question is at what  $\psi_1$  and  $\psi_2$  values to make wetting measurements. If possible, optimum values of  $\psi_1$  and  $\psi_2$  should be related to features that are identifiable on a graph. Such features include the point of maximum steepness of  $\theta_d(\psi)$  (where  $f$  is a maximum), symbolized  $\psi_{ms}$ ; the point of maximum curvature, symbolized  $\psi_{mc}$ , indicating approximately the air-entry value  $\psi_{ae}$ ; and the resaturation value  $\psi_{rs}$  (which is useful for discussion, though in practice it would not be known before the wetting measurements).

A brute force analysis of  $R^2$  as a function of  $\psi_1$  and  $\psi_2$  was useful in determining guidelines for selecting near-optimum locations of these points. Figure 9 shows one example of results of such computations. The maxima are quite broad, suggesting that the precise values of  $\psi_1$  and  $\psi_2$  are not very important as long as they are not in the distinctly off-maximum region. One rule of thumb, the taking of  $\psi_1$  at  $\psi_{ms}$  and  $\psi_2$  at  $0.9\psi_{mc}$ , produced high  $R^2$  values for nearly all of the media in Table 1. The position at  $\psi_{ms}$  is also intuitively attractive because it is a point where hysteresis is usually of great magnitude. The position at  $0.9\psi_{mc}$  is reasonable because it is off of  $\psi_{mc}$  in the direction of  $\psi_{rs}$ , but would seldom be in the nonhysteretic region between  $\psi_{rs}$  and zero. All the selected test media except for Plano silt loam and low-density silty sand were well modeled by these rules. The problem in the case of Plano silt loam is that  $\psi_{mc}$  has little significance when it is so close to zero. For this medium, and possibly for other undisturbed cores, both  $\psi_1$  and  $\psi_2$  should be to the left of  $\psi_{mc}$ . The problem with the low-density silty sand is that  $\theta_d(\psi)$  is so rounded where it departs from saturation that the value of  $\psi_{mc}$  is poorly determined. In this case  $\psi_1$  at  $\psi_{ms}$  works well, but  $\psi_2$  needs to be closer to zero, say at about  $0.7\psi_{mc}$ . A similar choice of  $\psi_2$  closer to zero would slightly improve the fit where air-entry is sharply defined but far from zero, as for Rubicon sandy loam.

For cases where only one measured point of the main wetting curve is available, either  $\nu$  or  $\beta$  could be estimated, based on general properties of the medium, and the other calculated to fit the known point.

Because whole classes of media may be representable by single  $\beta$  values and because of a greater sensitivity of modeled results to  $\nu$ , it would generally be best to estimate  $\beta$  and calculate  $\nu$ . An analysis based on the partial derivatives of the modeled  $\theta_w$  with respect to  $\nu$  and  $\beta$  demonstrated this greater sensitivity to  $\nu$ . Though it showed little about optimum locations for points to be measured, this analysis showed a clearly greater magnitude of the sensitivity to  $\nu$  than to  $\beta$ , especially for the more highly structured media. The ratio of  $\nu$  sensitivity to  $\beta$  sensitivity ranged from about 3 for glass beads and Plainfield sand to  $>100$  for Plano silt loam.

When wetting data are absent, it may be possible to estimate both  $\nu$  and  $\beta$  based on values determined for a related medium. It may also be possible eventually to relate them to other characteristics, for example  $\nu$  to a measured  $\theta$  at some extreme  $\psi$  value. It would be better to have means of measuring these parameters directly, though it may not be possible to do so in a way that is easier than measuring two wetting curve points.

After the drying and wetting main curves have been determined, the optimized  $\beta$  and  $\nu$  values can be computed and used to generate scanning curves using Eq. [5] and [8], and similar ones for higher orders. Alternatively, a model such as Mualem's (1974) may be used to compute scanning curves from the main curves.

## DISCUSSION AND CONCLUSIONS

The model presented here employs concepts of soil properties that have a definite physical interpretation, and parameters that are quantified empirically. It has practical value for computing hysteretic water relations from minimal data. It also has fundamental value to the extent that the parameter values can characterize certain features of a medium that determine the behavior of water in its pores.

The best support for the model is in the quality of the fits to the wetting curves, that they are (i) better than would be expected from a purely empirical two-parameter formula, and (ii) of high quality across a wide range of texture, structure, and other properties. This justification of the model strongly suggests that there is self-similarity in the distribution of nonhysteretic pore space with respect to pore size and that a pore-body-size distribution can be represented as a stretched-out version of the pore-neck-size distribution. While supported by the fits to measured data, these hypotheses are clearly imperfect. The self-similarity implied by constancy of  $\nu$  may sometimes break down for the largest pores, especially where the air-entry effect is unusually pronounced. In particular, the evidence suggests that the extent of self-similarity is reduced when natural soil structure is disturbed by artificial repacking. Allowing  $\nu$  to depend on  $\psi$  in some way might improve the model's versatility, at the expense of simplicity. Though possible modifications to the pore-size-distribution hypothesis are less obvious, there may be a way to relate body- and neck-size distributions that is simpler or produces better fits.

Of the two parameters,  $\nu$  exerts a greater influence

over the modeled curves than does  $\beta$ . With additional assumptions it may be possible to create a reasonable, though less accurate, model that has  $\nu$  as its sole parameter. Whether this is the objective or not, consideration of nonhysteretic pore space is a vital element in the creation of improved models of soil water hysteresis.

The model's practical usefulness lies mainly in the fact that fewer data are required for reasonable prediction of a hysteretic relation. Its chief strength is the accuracy of the main wetting curves it produces. It can also generate scanning curves, though in some cases it may be best to use this model to complete the main hysteresis envelope, then to use a domain model to generate the scanning curves. The calculations required by this new model are straightforward, though somewhat more complicated than for models currently in widespread use. The chief potential difficulty is in the need to differentiate a function defined by measured data points.

Values of the model's parameters provide quantitative information about porous media characteristics, including structure. The parameter  $\nu$ , representing pore space that water can occupy in the form of films, dead-end pores, narrow parts of pores, and similar structures, is related to smoothness and uniformity of particles and to degree of compaction. It is essentially zero for uniform, smooth, spherical beads, and has values between about 0.1 and 0.5 for more complicated particles. The body-to-neck ratio  $\beta$  seems to correlate most closely with soil structure. It has values between about 2.1 and 2.6 for media with little aggregation, between about 3 and 10 for repacked fine-textured media and consolidated media, and  $>10$  for a soil with a high degree of natural structure including aggregation and biologically induced macropores. The trends observed with both  $\nu$  and  $\beta$  values give hope that it may be possible to relate these parameters to easily observed features of a porous medium, thereby further reducing the effort required to quantify soil water hysteresis.

## REFERENCES

- Chen, Y., and M. Schnitzer. 1978. The surface tension of aqueous solutions of soil humic substances. *Soil Sci.* 125:7–15.
- Childs, E.C., and N. Collis-George. 1950. The permeability of porous materials. *Proc. R. Soc. London* 201A:392–405.
- Croney, D., and J.D. Coleman. 1954. Soil structure in relation to soil suction (pF). *J. Soil Sci.* 5:75–84.
- Donaldson, J.R., and P.V. Tryon. 1983. Nonlinear least squares regression using STARPAC. Tech. Note 1068-2. Natl. Bureau of Standards, Boulder, CO.
- Draper, N.R., and H. Smith. 1981. Applied regression analysis. 2nd ed. John Wiley & Sons, New York.
- Enderby, J.A. 1955. The domain model of hysteresis. Part 1 — Independent domains. *Trans. Faraday Soc.* 51:835–848.
- Everett, D.H. 1955. A general approach to hysteresis. Part 4. An alternative formulation of the domain model. *Trans. Faraday Soc.* 51:1551–1557.
- Fritsch, F.N., and J. Butland. 1984. A method for constructing local monotone piecewise cubic interpolants. *SIAM J. Sci. Stat. Comput.* 5:300–304.
- Haines, W.B. 1930. Studies in the physical properties of soil. V. The hysteresis effect in capillary properties and the modes of water distribution associated therewith. *J. Agric. Sci. (Cambridge)* 20:97–116.
- Miller, E.E., and R.D. Miller. 1956. Physical theory for capillary flow phenomena. *J. Appl. Phys.* 27:324–332.
- Mualem, Y. 1973. Modified approach to capillary hysteresis based on a similarity hypothesis. *Water Resour. Res.* 9:1324–1331.
- Mualem, Y. 1974. A conceptual model of hysteresis. *Water Resour. Res.* 10:514–520.
- Mualem, Y. 1977. Extension of the similarity hypothesis used for modeling the soil water characteristics. *Water Resour. Res.* 13:773–780.
- Mualem, Y. 1984. Prediction of the soil boundary wetting curve. *Soil Sci.* 137:379–390.
- Mualem, Y., and G. Dagan. 1975. A dependent domain model of capillary hysteresis. *Water Resour. Res.* 11:452–460.
- Néel, L. 1942. Theories des lois d'aimantation de Lord Rayleigh. 1. *Cah. Phys.* 12:1–20.
- Néel, L. 1943. Theories des lois d'aimantation de Lord Rayleigh. 2. *Cah. Phys.* 13:18–30.
- Nimmo, J.R. 1983. The temperature dependence of soil-water characteristics. Ph.D. diss. Univ. of Wisconsin, Madison (Diss. Abstr. 83-17041).
- Nimmo, J.R., and E.E. Miller. 1986. The temperature dependence of isothermal water vs. pressure characteristics of soils. *Soil Sci. Soc. Am. J.* 50:1105–1113.
- Parlange, J.-Y. 1976. Capillary hysteresis and the relationship between drying and wetting curves. *Water Resour. Res.* 12:224–228.
- Philip, J.R. 1964. Similarity hypothesis for capillary hysteresis in porous materials. *J. Geophys. Res.* 69:1553–1562.
- Poulovassilis, A. 1962. Hysteresis of pore water, an application of the concept of independent domains. *Soil Sci.* 93:405–412.
- Press, W.H., B.P. Flannery, S.A. Teukolsky, and W.T. Vetterling. 1989. Numerical recipes. Cambridge Univ. Press, New York.
- Staple, W.J. 1965. Water tension, diffusivity, and conductivity of a loam soil during wetting and drying. *Can. J. Soil Sci.* 45:78–86.
- Stonestrom, D.A. 1987. Co-determination and comparisons of hysteresis-affected, parametric functions of unsaturated flow: Water-content dependence of matric pressure, air-trapping, and fluid permeabilities in a non-swelling soil. Ph. D. diss. Stanford Univ., Stanford, CA (Diss. Abstr. 88-01040).
- Topp, G.C. 1969. Soil water hysteresis measured in a sandy loam compared with the hysteretic domain model. *Soil Sci. Soc. Am. Proc.* 33:645–651.
- Topp, G.C. 1971. Soil water hysteresis in silt loam and clay loam soils. *Water Resour. Res.* 7:914–920.
- Toledo, P.G., R.A. Novy, H.T. Davis, and L.E. Scriven. 1990. Hydraulic conductivity of porous media at low water content. *Soil Sci. Soc. Am. J.* 54:673–679.
- Tschapek, M., C.O. Scoppa, and C. Wasowski. 1978. The surface tension of soil water. *J. Soil Sci.* 29:17–21.
- Tyler, S.W., and S.W. Wheatcraft. 1989. Application of fractal mathematics to soil water retention estimation. *Soil Sci. Soc. Am. J.* 53:987–996.

# ERRATUM

## Semiempirical Model of Soil Water Hysteresis

JOHN R. NIMMO

*Soil Sci. Soc. Am. J.* 56:1723-1730 (November-December 1992)

On p. 1725, the captions for Fig. 3 and 4 are interchanged. Figure 4, the key diagram illustrating the formulation of the model, should appear with its caption as follows.

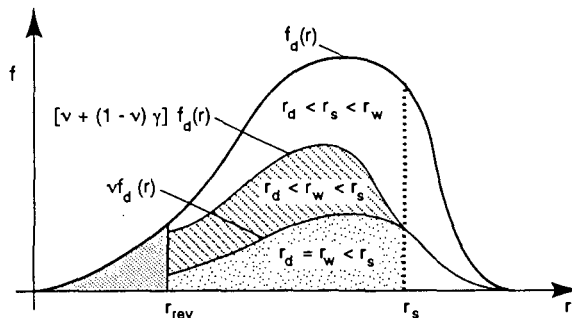


**Fig. 4.** Diagram illustrating the application of the model to the situation existing after drying to  $r_{rev}$  and then rewetting to  $r_s$ . The water content for this condition is proportional to the sum of the three shaded areas: the gray area that never was emptied, the dotted area with nonhysteretic space that refills at the same  $r$  values at which it emptied, and the hatched area with hysteretic space that refills at  $r \leq r_s$ .